Published in final edited form as:
J Med Primatol. 2010 October ; 39(5): 356–360. doi:10.1111/j.1600-0684.2010.00416.x.

AIDS and optic neuritis in a rhesus monkey infected with the R5 clade C SHIV-1157ipd3N4

Ana Patricia Garcia[1,2,*], **Nagadenahalli B. Siddappa**[3,4], **Qingsheng Li**[5], **Ashley T. Haase**[5], **Katherine Paul**[6], **Fawn Stroud**[1], **Xiaodong Zhang**[1], **Jack A. Fountain**[7], **Francois Villinger**[1,2], **Francis J. Novembre**[1], **James G Else**[1], **W. Evan Secor**[6], and **Ruth M. Ruprecht**[3,4,*]

[1] Yerkes National Primate Research Center, Emory University, Atlanta, Georgia, USA

[2] Department of Pathology & Laboratory Medicine, School of Medicine, Emory University, Atlanta, Georgia, USA

[3] Dana-Farber Cancer Institute, Boston, Massachusetts, USA

[4] Harvard Medical School, Boston, Massachusetts, USA

[5] Department of Microbiology, School of Medicine, University of Minnesota, Minneapolis Minnesota, USA

[6] Centers for Disease Control and Prevention, Atlanta, Georgia, USA

[7] Department of Radiology, School of Medicine, Emory University, Atlanta, GA

Abstract

A Chinese rhesus macaque infected with the pathogenic CCR5-tropic clade C simian-human immunodeficiency virus, SHIV-1157ipd3N4, had persistent viremia, depletion of $CD4^+$ T cells to <200 cells/μl, opportunistic infections, coagulopathy and gradual development of bilateral blindness. MRI revealed marked thickening of both optic nerves. Histopathological evaluation showed diffuse cellular infiltration at necropsy, and a focus of infected cells. This is the first report of CNS pathology following chronic infection with an obligate R5 SHIV.

Keywords

R5 SHIV; neuroAIDS; optic neuropathy

Introduction

Worldwide, human immunodeficiency virus type 1 (HIV-1) clade C accounts for more than 56% of all cases of HIV-1/AIDS (www.UNAIDS.org). To study HIV-1 pathogenesis and vaccine efficacy, several simian-human immunodeficiency viruses (SHIVs) encoding HIV-1 *env* genes in SIVmac239 backbones have been developed (reviewed in [9]). We have generated a series of CCR5-tropic SHIVs encoding *env* genes of primary HIV-1 clade C strains isolated early after mother-to-child transmission [5, 6, 8]. One isolate, SHIV-1157i, has been passaged rapidly through infant rhesus monkeys (RM); after AIDS developed in the first RM, we reisolated an infectious molecular clone, SHIV-1157ipd3N4 [8]. Here we

Correspondence: Anapatricia Garcia D.V.M., Ph.D., Yerkes National Primate Research Center, Emory University, Atlanta, Georgia, USA, Department of Pathology & Laboratory Medicine, School of Medicine, Emory University, Atlanta, Georgia, USA, agarci5@emory.edu, Ruth M. Ruprecht, M.D., Ph.D., Dana-Farber Cancer Institute, Boston, Massachusetts, USA, Harvard Medical School, Boston, Massachusetts, USA, Ruth_Ruprecht@dfci.harvard.edu.

describe a Chinese-origin RM with chronic SHIV-1157ipd3N4 viremia, progression to AIDS with multiple opportunistic infections and neurologic symptoms. To our knowledge, this is first report of CNS pathology following chronic infection with SHIV using only R5 in vivo.

Case Report

An adult female Chinese-origin RM (RQ3911) was acquired by and maintained at the Centers for Disease Control and Prevention (CDC) in accordance with the Animal Care and Use Committee (ACUC). The monkey was inoculated intrarectally with SHIV-1157ipd3N4 as part of a study examining the influence of *Schistosoma mansoni* coinfection on host susceptibility to R5 SHIV; RQ3911 was part of the parasite-free control group [1]. Peak viremia occurred at week 2 post-inoculation (pi) (Fig. 1A); RQ3911 seroconverted within 12 weeks pi (data not shown). The animal was persistently viremic with viral RNA loads ranging between 10^4 to 5×10^6 copies/ml (Fig. 1A). Absolute peripheral blood $CD4^+$ T cells were gradually depleted (Fig. 1A); the fraction of $CD4^+CD29^+$ memory T cells declined to abnormal levels in parallel (Fig. 1B). The animal developed clinical AIDS as defined by $CD4^+$ T cell <200 cells/μl was diagnosed at about 2 years p.i. At approximately 1 year pi, the animal also developed thrombocytopenia (Fig. 1B) that remained clinically unremarkable until late in the course of disease.

Approximately 33 months pi, the animal experienced bloody diarrhea and appeared to have vision problems. On examination, the right pupil was fixed and dilated and the left pupil was constricted. Gradual weight loss was also noted, and the RM was given fluids and treated with BaytrilR. Stool culture was negative. One month later, abdominal distension was noted; additional clinical findings included gingivitis, enlarged axillary and inguinal lymph nodes, decreased extension of the right knee as well as constricted pupils with bilateral blindness. During funduscopic exam, the optic disks were difficult to visualize and only few blood vessels were visible. Rectal and gingival swabs were obtained for culture and fluids were given. The most significant hematologic findings were anemia, lymphocytopenia and thrombocytopenia. The monkey was transferred to the Yerkes Primate Center to undergo MRI examination and based upon poor prognosis, was subsequently euthanized.

MRI studies were performed on the anesthetized monkey using a clinical scanner (Siemens Trio 3T, Malvern, PA) with the Extremity CP knee coil. The RM was placed in the sphinx position in the scanner with the head immobilized in a home-built holder. The MRI pulse sequences included: 1) T1-weighted magnetization-prepared gradient-echo (MP-RAGE) anatomical images and 2) T2-weighted fast spin-echo images. MRI findings included enlargement of both optic nerves sheaths with an infiltrative, uniform pattern obscuring the nerve (Fig. 2B-D); the globes did not appear to be infiltrated. There was a low-intensity soft-tissue signal on T1 and T2 within the orbits surrounding the optic nerve sheath and extending from the orbital apex to the back of the globe (Fig. 2C), suggesting marked cellular infiltration of the normally bright appearing fat tissue on T1 (Fig.2A): The superior orbital veins appeared patent but the extraocular muscles could not be delineated within the orbit due to the uniform low signal of the orbital fat and muscle (Fig. 2A vs B). These findings were most consistent with a cellular infiltrate with high nuclear to cytoplasm ratios, as is seen in lymphoma, leukemia, or similar small cell processes such as an anti-infective response.

Following MRI, the RM was euthanized, perfused with phosphate-buffered saline (PBS), and submitted to postmortem examination. The stomach mucosa was diffusely reddened. The small intestinal and rectal mucosae were diffusely thickened, reddened and irregular. The mucosa of the urinary bladder had multifocal petechial to ecchymotic hemorrhages. The

inguinal, axillary and mesenteric lymph nodes were markedly enlarged. Both lungs had a red, mottled appearance. The pulmonary valves had multifocal small raised nodules, consistent with a vegetative lesion. The right A-V valve had small vegetations ranging from 10–20 mm and the right ventricle contained a mural thrombus (Fig. 1C). The cervical muscles at the level of C1-C3 had a focal area of hemorrhage; at this level, the meninges of the spinal cord segment were also hemorrhagic. The optic nerves were grossly enlarged. The caudal aspect of the right eye, adjacent to the optic nerve, had a raised firm nodule.

Cardiac blood and thrombus specimens were collected aseptically for bacterial culture; *Streptococcus* spp. were isolated. Sections of all major organs were collected for routine histopathological evaluation and in situ hybridization (ISH). In addition, both eyes including the optic nerves were removed and preserved in Bouin's solution (Sigma-Aldrich, St. Louis, MO). Histologic evaluation of the optic nerves revealed severe infiltration of neutrophils in both nerves, sclera, as well as in the medial, superior and lateral rectus muscles. Rare spindle cells exhibited karyomegaly and often contained intranuclear inclusions (INIB) consistent with cytomegalovirus (CMV) infection (Fig. 1E). Immunohistochemistry (IHC) with a polyclonal rabbit anti-rhesus CMV (gift of Dr. P.A. Barry, UC Davis) was weakly positive in endothelium of occasional blood vessels (data not shown). However, IHC for CMV was negative in areas with INIB, potentially due to control of active CMV replication at this site by the time of euthanasia. Multifocal areas of fibrovascular proliferation and variable size areas of lymphocytic infiltration were also intermixed with the purulent infiltration. However, special stains for bacterial, fungal and acid fast bacteria were all negative in the optic nerve. The meninges of the cervical spinal cord (C1-C3) had a focally extensive area of hemorrhage that extended to the adjacent neuropil. Histopathology of the cerebral cortex showed diffuse astrocytosis and astrogliosis (Figure 1F) with a hypoplastic molecular (zonal layer or plexiform layer of Cajal) layer in some areas; many neurons were markedly pyknotic. In addition to neurologic lesions, histological examination of other organs revealed pulmonary hemorrhage, adenoviral enteritis and ulcerative gastritis with severe neutrophilic infiltration (Fig. 1D) intermixed with gram negative bacterial rods and rare eosinophilic INIB, consistent with CMV infection.

ISH for SIV *gag* RNA was performed on paraffin-embedded optic nerve and formalin-fixed brain sections (mid-frontal cortex, brain stem and cerebrum) 11]. ISH revealed clusters of virus-infected cells in the optic nerve (Fig. 1G) and in the mid-frontal cortex (Fig. 1H); ISH was negative in tissues of the brain stem and cerebrum.

Discussion

Here we have shown with the case of RM RQ3911 that 1) chronic infection with the R5 SHIV-1157ipd3N4 caused persistent viremia and gradual progression to AIDS; 2) clinical signs included thrombocytopenia, diarrhea and gradual weight loss as well as bilateral blindness; 3) AIDS was associated with multiple infections, including vegetative endocarditis, adenoviral enteritis, and severe bilateral optic neuritis. The latter was associated with infiltration of cells productively infected with SHIV-1157ipd3N4 as well as cells with intranuclear inclusions and karyomegaly consistent with CMV neuritis; 4) diffuse cerebral involvement was characterized by astrocytosis and rare SIV *gag*-positive cells by ISH; and 5) hemorrhage in some organs.

HIV-1 infection is known to cause neurologic disease in humans, where productive viral replication in the CNS coincides with marked depletion of peripheral $CD4^+$ T cells. However, the specific mechanisms of neuroAIDS remain to be fully elucidated. In patients with AIDS, loss of cortical neurons and optic nerve axons has been reported [4]. However, loss of optic nerve axons was not observed in RQ3911; rather, lymphocytic aggregates and

fibrovascular proliferation in the optic nerves suggest indirect pathology due to a chronic viral process consistent with the blindness prior to euthanasia. Optic neuritis in our monkey could have been mediated directly by SHIV-infected mononuclear cells or macrophages. However, we did not observe the typical hallmarks of HIV-1 AIDS dementia in humans or SIV encephalitis in monkeys, namely perivascular mononuclear cuffing, formation of microglial nodules or multinucleated giant cells [2, 3, 10]. Although SIV *gag* RNA was detected by ISH in the optic nerves and mid-frontal cortex, the level of productive SHIV infection in this compartment remained modest. Probably, SHIV-1157ipd3N4 as well as CMV were linked to the development of optic neuritis in this animal. Microscopically, CMV lesions were found in organs of the central and peripheral nervous, lymphatic, vascular, digestive and reproductive systems. The histological hallmark of the lesion induced by the virus is intranuclear and intracytoplasmic inclusion bodies, cytomegaly and neutrophilic infiltration [7], features observed in the present case. Furthermore, since CMV infection is known to induce the host cells to express proinflammatory proteins, such as IL-8 and RANTES, and also other binding molecules, such as ICAM-1 and LFA-3, recruitment and aggregation of neutrophils at the site of the lesion is very common and characteristic of a CMV infection [7]. Additional studies are underway to elucidate the pathogenesis of neuro-ophthalmological disorders associated with our CCR5-tropic Clade C SHIV. To our knowledge, this is the first report of neuritis associated with SHIV infection targeting CCR5 exclusively in a rhesus monkey, since dual tropic SHIV predominantly use CXCR4 in vivo [12].

Acknowledgments

The authors would like to thank Dr. Peter A. Barry (University of California, Davis) for the kind gift of rabbit anti-monkey CMV antiserum; Drs. Prachi Sharma and Daniel Anderson (YNPRC) for their help in the evaluation of the case including CMV IHC; Dr. Larry Walker (YNPRC) for submitting normal control MRI images and Eileen Breding and Evan Dessasau for excellent technical assistance. The work was supported by NIH grants R56 AI062515 to R.M.R., PO1 AI 048240 to R.M.R. and J.G.E., and base grant RR-000165 to the Yerkes National Primate Research Center.

References

1. Chenine AL, Shai-Kobiler E, Steele LN, Ong H, Augostini P, Song R, Lee SJ, Autissier P, Ruprecht RM, Secor WE. Acute Schistosoma mansoni infection increases susceptibility to systemic SHIV clade C infection in rhesus macaques after mucosal virus exposure. PLoS Negl Trop Dis. 2008; 2:e265. [PubMed: 18648516]
2. Clements JE, Mankowski JL, Gama L, Zink MC. The accelerated simian immunodeficiency virus macaque model of human immunodeficiency virus-associated neurological disease: From mechanism to treatment. J Neurovirol. 2008; 14:309–17. [PubMed: 18780232]
3. Fischer-Smith T, Bell C, Croul S, Lewis M, Rappaport J. Monocyte/macrophage trafficking in acquired immunodeficiency syndrome encephalitis: Lessons from human and nonhuman primate studies. J Neurovirol. 2008; 14:318–26. [PubMed: 18780233]
4. Goldsmith P, Jones RE, Ozuzu GE, Richardson J, Ong EL. Optic neuropathy as the presenting feature of HIV infection: Recovery of vision with highly active antiretroviral therapy. Br J Ophthalmol. 2000; 84:551–3. [PubMed: 10847713]
5. Humbert M, Rasmussen RA, Song R, Ong H, Sharma P, Chenine AL, Kramer VG, Siddappa NB, Xu W, Else JG, Novembre FJ, Strobert E, O'Neil SP, Ruprecht RM. SHIV-1157i and passaged progeny viruses encoding R5 HIV-1 clade C env cause AIDS in rhesus monkeys. Retrovirology. 2008; 5:94. [PubMed: 18928523]
6. Siddappa NB, Song R, Kramer VG, Chenine AL, Velu V, Ong H, Rasmussen RA, Grisson RD, Wood C, Zhang H, Kankasa C, Amara RR, Else JG, Novembre FJ, Montefiori DC, Ruprecht RM. Neutralization-sensitive R5-tropic simian-human immunodeficiency virus SHIV-2873Nip, which carries env isolated from an infant with a recent HIV clade C infection. J Virol. 2009; 83:1422–32. [PubMed: 19019970]

7. Sinclair J. Human cytomegalovirus: Latency and reactivation in the myeloid lineage. J Clin Virol. 2008; 41:180–185. [PubMed: 18164651]

8. Song RJ, Chenine AL, Rasmussen RA, Ruprecht CR, Mirshahidi S, Grisson RD, Xu W, Whitney JB, Goins LM, Ong H, Li PL, Shai-Kobiler E, Wang T, McCann CM, Zhang H, Wood C, Kankasa C, Secor WE, McClure HM, Strobert E, Else JG, Ruprecht RM. Molecularly cloned SHIV-1157ipd3N4: A highly replication- competent, mucosally transmissible R5 simian-human immunodeficiency virus encoding HIV clade C env. J Virol. 2006; 80:8729–38. [PubMed: 16912320]

9. Vlasak J, Ruprecht RM. AIDS vaccine development and challenge viruses: Getting real. Aids. 2006; 20:2135–40. [PubMed: 17086052]

10. Williams R, Bokhari S, Silverstein P, Pinson D, Kumar A, Buch S. Nonhuman primate models of neuroaids. J Neurovirol. 2008; 14:292–300. [PubMed: 18780230]

11. Zhang Z, Schuler T, Zupancic M, Wietgrefe S, Staskus KA, Reimann KA, Reinhart TA, Rogan M, Cavert W, Miller CJ, Veazey RS, Notermans D, Little S, Danner SA, Richman DD, Havlir D, Wong J, Jordan HL, Schacker TW, Racz P, Tenner-Racz K, Letvin NL, Wolinsky S, Haase AT. Sexual transmission and propagation of SIV and HIV in resting and activated CD4+ T cells. Science. 1999; 286:1353–7. [PubMed: 10558989]

12. Goodnow MM, Collman RG. HIV-1 coreceptor preference is distinct from target cell tropism: a dual-parameter nomenclature to define viral phenotypes. J Leuk Biol. 2006; 80:965–72.

A. vRNA loads and CD4$^+$ T cells

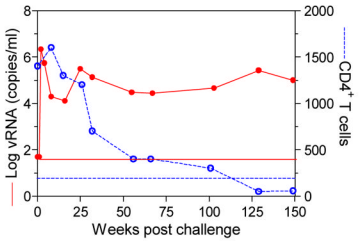

B. CD4$^+$CD29$^+$ T cells and platelets

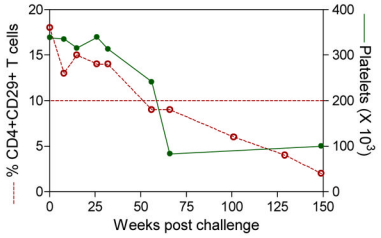

C. Vegetative endocarditis with mural thrombus

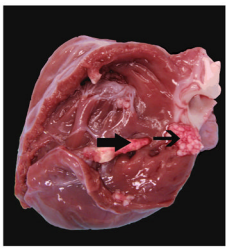

D. Proximal stomach, intranuclear inclusion ,

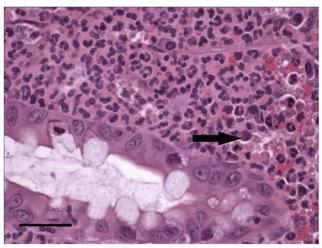

E. Optic nerve karyomegalic inclusion

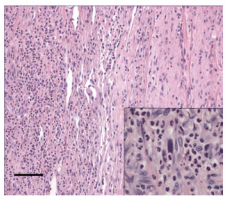

F. Astrogliosis in the cerebrum

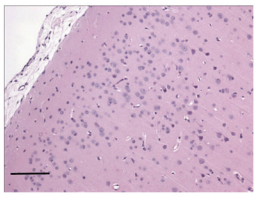

G.. Optical nerve ISH for SIV *gag* RNA

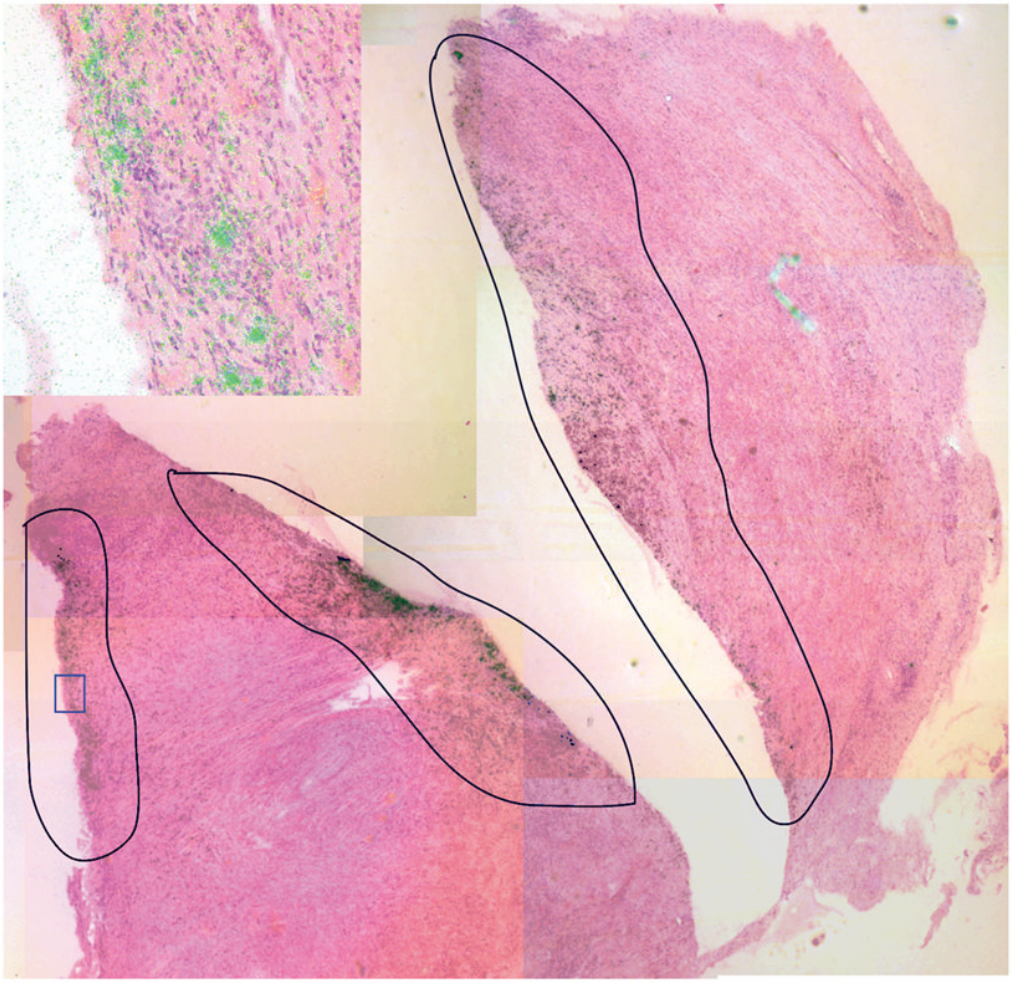

H. ISH on mid-frontal cortex

Fig. 1.

Disease progression and pathologic findings of RQ3911. (A) Viral loads and absolute $CD4^+$ T-cell counts; (B) percentage of memory $CD4^+CD29^+$ T cells; (C) picture of vegetative endocarditis (arrow) and thrombus (arrow head); (D) photomicrograph of purulent infiltration and intranuclear inclusion of the proximal stomach (arrow). Bar = 100 μm; (E) photomicrograph of the optic nerve depicting inflammatory response and karyomegalic inclusion (insert). Bar = 100 μm; (F) Photomicrograph of cerebral cortex depicting astrogliosis. Bar = 180 μm; (G) Montage image with SIV RNA+ cells detected by ISH in encircled areas. In transmitted light, the infected cells appear black. In reflected light, the SIV RNA+ cells in the enlarged inset indicated by the blue rectangle appear green. (H) SIV RNA+ cell in mid-frontal cortex. The tissue in the insert with the blue background is a positive ISH control.

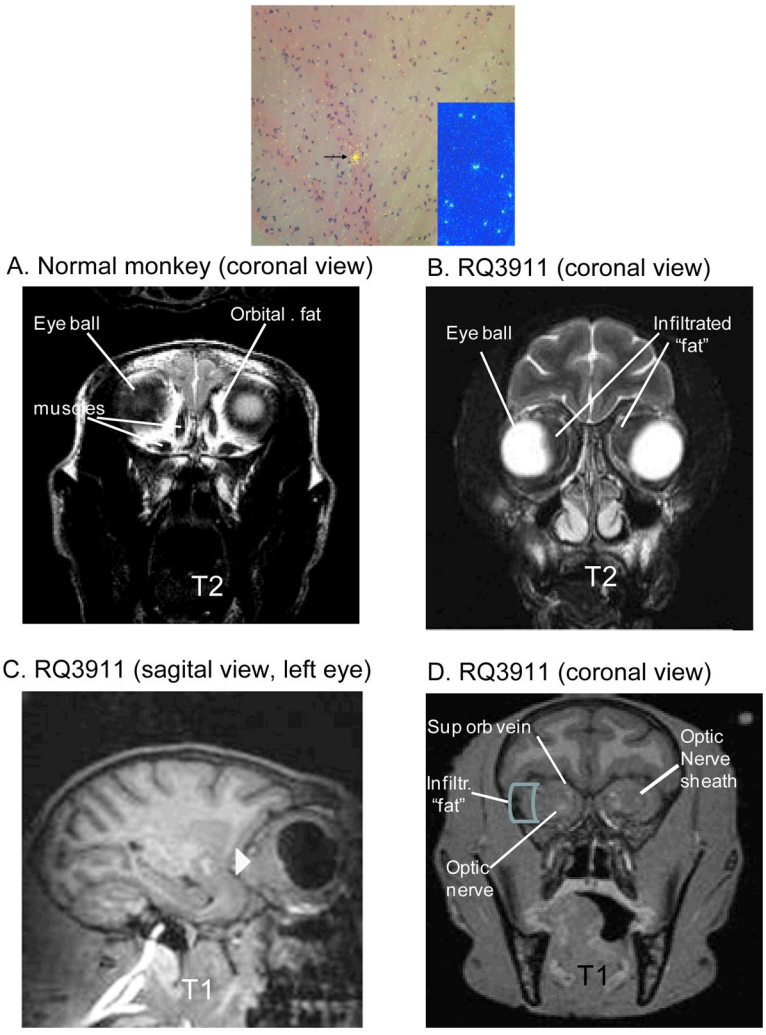

Fig. 2.

(A) Normal RM and (B-D) monkey RQ3911 with bilateral enlargement of both optic nerve sheaths. (A,B) T2-weighted scans (TR = 5040 ms, TE = 115 ms, FOV = 128 mm × 128 mm, data matrix = 256 × 256, turbo factor = 17, slice thickness = 2 mm, total 34 slices, 4 averages) showing the dense intraconal mass surrounding the optical nerve and blurring the resolution of the supraorbital vein, orbital nerve and extraorbital muscles (A) into a single non-descript mass (B). (C,D) T1-weighted MRI (TR=2500 ms, TE=3.33 ms, FOV=116 mm × 116 mm, flip angle= 8 degrees, TI=950 ms, matrix = 192 × 192, slice thickness = 0.6 mm, 144 slices, 6 averages) showing the intraorbital periocular mass (arrow head in C), and "gated" infiltrated mass. (D) A vitamin E capsule marker indicates right side in the upper right corner. The control monkey shown in (A) was taken from the Yerkes archive, and although the analysis had the animal's head at a slightly different angle, the control picture shows the orbital area at the same level of neoptic nerve entry for comparison.